Research Article Vol. 40, No. 8 / August 2023 / Journal of the Optical Society of America A 1527

Journal of the Optical Society of America A
OPTICS, IMAGE SCIENCE, AND VISION

Effects of different cladding materials on orbital angular momentum modes propagating in photonic crystal fibers

Ning Sheng,[1] Haihao Fu,[1] Tongyu Meng,[2] Jianxin Wang,[1] Wei Liu,[1] Jingwei Lv,[1] Zao Yi,[3] Lin Yang,[1] Paul K. Chu,[4] and Chao Liu[1,*]

[1]School of Electronics Science, Northeast Petroleum University, Daqing 163318, China
[2]Leicester International Institute, Dalian University of Technology, Dalian 124221, China
[3]Joint Laboratory for Extreme Conditions Matter Properties, Southwest University of Science and Technology, Mianyang 621010, China
[4]Department of Physics, Department of Materials Science and Engineering, and Department of Biomedical Engineering, City University of Hong Kong, Tat Chee Avenue, Kowloon, Hong Kong, China
*msm-liu@126.com

Received 11 April 2023; revised 11 June 2023; accepted 18 June 2023; posted 3 July 2023; published 17 July 2023

With the development of orbital angular momentum (OAM) photonic crystal fibers (PCFs) for more efficient communication, fiber claddings are important to the performance. In this paper, the influence of SiO_2 and four new optical materials, which are amethyst, SSK2, SF11, and LaSF09, as cladding materials, on the OAM mode characteristics is studied based on a common PCF for OAM transmission. In addition, the effective index difference, dispersion, confinement loss, and other properties of OAM modes transmitted in the five materials are derived by the finite element method. After in-depth analysis, universal rules can be obtained as guidelines for optimization of PCF in the future for improving the efficiency of optical fiber communication. Through chart analysis, it can be concluded that when materials of high effective refractive indices are used as cladding materials for PCF, the dispersion, nonlinear coefficient, confinement loss, mode purity, and other properties are significantly improved. Lower dispersion and confinement loss are more conducive to long-distance communication transmission. The decrease in nonlinear coefficient represents a better effect in suppressing nonlinear effects, and the increase in numerical aperture and mode purity respectively improves the transmission efficiency and stability of OAM communication. These conclusions provide universal rules for high-quality communication in the future.

https://doi.org/10.1364/JOSAA.492898

1. INTRODUCTION

With the rapid development of Internet technology, modern communication has put forward increasingly high requirements for high-capacity and efficient information transmission. Optical communication is a technology with light wave as the carrier, which can convert other signals into optical semaphores for information transmission [1,2]. Compared with traditional communication methods, it has been widely used due to its advantages such as long relay distance, strong anti-interference ability, and low cost [3]. Optical fiber communication is a new method of optical communication. By selecting the appropriate multiplexing mode, the optical signal is coupled into the optical fiber for transmission. There are many multiplexing methods for signal coupling, such as frequency-division multiplexing [4], time-division multiplexing [5], etc., but these multiplexing methods cannot circumvent the Shannon limit [6] when transmitting information in single-mode fibers [7–9]. The mode-division multiplexing (MDM) [10] technology adopts the mode of multiple input and multiple output to increase the amount of signals transmitted in each optical fiber which can construct a multiplex system on the same spectral channel. In addition, the orbital angular momentum (OAM) in vortex light which has spiral phase wavefront $\exp(il\varphi)$ is a natural property of light [11–14], where φ is the azimuth angle, and l is the topological charge that can be any integer between negative infinity and positive infinity theoretically. For the reason that the vortex light carrying different topological charges of OAM are orthogonal to each other, OAM has an infinite number of orthogonal bases and can be used for MDM, which has great potential in optical communication. If these orthogonal bases are used as independent channels for information transmission by the MDM technology, the communication capacity of optical fibers can be improved greatly [15]. However, traditional single-mode or multimode fibers cannot carry the propagation of OAM modes because of uncontrollable dispersion and low

refractive index difference between related eigenmodes, so a new type of optical fibers must be selected to transmit them.

Photonic crystal fibers (PCFs) can freely adjust structural parameters and provide more flexible design, which meet the conditions required for OAM transmission. In recent years, many PCFs with excellent performance have been proposed to transmit OAM modes [16–21]. For example, Wan *et al.* [22] have designed a PCF which can transmit 30 OAM modes and proposed two methods to reduce dispersion and confinement loss by improving the structure of the original PCF. Zhang *et al.* [23] have devised a ring PCF which can support stable propagation of 30 OAM modes and analyzed the effects of pore ovalization. The eigenmode has higher purity and lower cross talk. Fu *et al.* [24] have utilized a simple PCF to explore the influence of the shape, size, number, spacing, and other parameters of the cladding pores on the dispersion and confinement loss and optimize the properties.

The materials used in these structures are invariably SiO_2 ($n = 1.444$ when the wavelength is 1.55 μm) and high-refractive-index rings of other materials are embedded in the annular region. Although SiO_2 is cheap, it has limitations in transmission performance. SiO_2 cannot meet the demand when higher requirements are proposed. Embedding high-refractive-index rings makes the structural design and actual production complex and the available production process cannot achieve precise manufacturing of it. Consequently, in order to improve the efficiency and performance of optical fiber communication and reduce the structural complexity, it is crucial to identify more suitable materials for optical fibers. Fu *et al.* [25] have designed a circular PCF composed of inlaid amethyst to support transmission of 118 OAM modes. Kolyadin *et al.* [26] have compared and analyzed the dispersion characteristics of the hollow-core PCF and negative curvature hollow-core fibers and added different blocks of SF11 glass to compress the pulses at the fiber output to obtain anomalous dispersion.

This work chooses four new optical materials with high refractive index that can be used for transmitting OAM modes in PCF. The finite element method is used to calculate the effective index difference, dispersion, nonlinear coefficient, mode purity, numerical aperture (NA), walk-off length, confinement loss, and other properties of OAM modes under these four different cladding materials and SiO_2 at 1.55 μm using a simple PCF. The numerical simulated results indicate that when high-refractive-index materials are used as cladding materials, the transmission performance of PCF is significantly improved compared to SiO_2. Using charts to deeply analyze the impact of different materials on various properties and summarize relevant laws which can serve as a significant reference for design of PCF and OAM mode performance optimization in the future.

In the second section, the paper describes the fundamental theory of OAM modes transmitting in PCF in detail. Then five different cladding materials, the structure of the designed PCF, and the optimization process are introduced. The production method and process of PCF are also mentioned. In the third section, the work discusses the impact of PCF under different cladding materials on the OAM modes and summarizes the relevant laws. The impact of changes in structural parameters on transmission performance of the proposed PCF in production is evaluated. Then, the paper provides a table that compares the OAM communication performance of the devised PCF with other related reports.

2. FUNDAMENTAL THEORY AND PCF DESIGN

The mode in the optical fiber is a manifestation of spatial electromagnetic field distribution [27]. There are four eigenvector modes—TE mode, TM mode, HE mode, and EH mode—in the general circular symmetric fiber waveguide structure. The OAM mode is formed by linear superposition of the odd and even modes of the eigenvector mode HE or EH with the same order [28]. The transverse electric field distribution of the eigenvector mode in the polar coordinate system is expressed by Eq. (1) [29]:

$$\begin{cases} \mathrm{HE}^{\mathrm{even}}_{l+1,m} = F_{l,m}(r)\cdot(\hat{x}\cos(l\theta) - \hat{y}\sin(l\theta)) \\ \mathrm{HE}^{\mathrm{odd}}_{l+1,m} = F_{l,m}(r)\cdot(\hat{x}\sin(l\theta) + \hat{y}\cos(l\theta)) \\ \mathrm{EH}^{\mathrm{even}}_{l-1,m} = F_{l,m}(r)\cdot(\hat{x}\cos(l\theta) + \hat{y}\sin(l\theta)) \\ \mathrm{EH}^{\mathrm{odd}}_{l-1,m} = F_{l,m}(r)\cdot(\hat{x}\sin(l\theta) - \hat{y}\cos(l\theta)) \end{cases}, \tag{1}$$

where $F_{l,m}(r)$ is the radial field distribution of scalar LP mode and θ is the azimuth coordinate. Due to the complete degeneracy of the odd and even modes of the eigenmodes, they are expressed as a set of linear combinations according to Eq. (2):

$$\begin{cases} \left\{\vec{e}_{r;l,m}\right\} = \mathrm{HE}^{\mathrm{even}}_{l+1,m} \pm i\mathrm{HE}^{\mathrm{odd}}_{l+1,m} = F_{l,m}(r)\,\hat{\sigma} \pm \exp(\pm il\theta) \\ \left\{\vec{e}_{r;l,m}\right\} = EH^{\mathrm{even}}_{l-1,m} \pm iEH^{\mathrm{odd}}_{l-1,m} = F_{l,m}(r)\,\hat{\sigma} \pm \exp(\pm il\theta) \end{cases}. \tag{2}$$

Equation (3) represents the superposition process of OAM modes. When the effective index difference is greater than 1×10^{-4} between HE and EH modes of the same order, the OAM modes formed by vector mode superposition can stably transmit in the PCF. This is because HE and EH modes can be well separated when the effective index difference is greater than 1×10^{-4}, avoiding mode coupling. Inter-mode cross talk is greatly suppressed, making OAM modes transmitting in the PCF more stable. Mode coupling cannot be avoided when the effective index difference is less than 1×10^{-4}, leading to the degradation of the OAM mode to the LP mode, and the large increase in inter-symbol interference is not conducive to signal transmission [30]:

$$\begin{aligned} \mathrm{OAM}^{\pm}_{\pm l,m} &= \mathrm{HE}^{\mathrm{even}}_{l+1,m} \pm iHE^{\mathrm{odd}}_{l+1,m}, \\ \mathrm{OAM}^{\mp}_{\pm l,m} &= EH^{\mathrm{even}}_{l-1,m} \pm iEH^{\mathrm{odd}}_{l-1,m}, \end{aligned} \tag{3}$$

where l is the topological charge which can be taken as an integer, m represents the radial mode order which is usually 1 for reducing the difficulty of demultiplexing, "even" and "odd" represent the even or odd mode, the subscript "±" represents the spin state of the OAM mode, and "±" in front of l implies the right or left wavefront rotation direction. Accordingly, the number of OAM modes which are transmitted in the PCF can be calculated as follows. When $l = 1$, the EH modes cannot be synthesized into OAM and thus exist as two channels. If $l \geq 2$, there are four independent information states in the PCF and consequently, the total number of OAM modes which can be transmitted in the PCF is $l \times 4 + 2$ [31].

The OAM beam has a helical phase front $\exp(\pm il\Phi)$ (Φ is the azimuth angle). The OAM modes of different orders are orthogonal to each other, which can be infinite modes in theory [32]. When OAM is transmitted in the PCF as an information carrier, the transmitted information is converted into an optical signal at the transmitting end and modulated into the laser beam emitted by the laser, so that the photon intensity changes with the frequency of the optical signal transmitted in the PCF based on the principle of total internal reflection. The receiving terminal accepts the optical signal, converts it into an electrical signal, and deciphers the transmitted information by demodulation. The OAM modes superimposed by vector modes can be stably transmitted in the PCF when the effective refractive index difference is greater than 1×10^{-4} [33–35].

At present, PCF produced by a variety of materials can support transmission of OAM modes. The distinct refractive index of these materials enables diverse performance of OAM modes transmitted in the PCF. In order to study the effects on the supported OAM modes for materials with various effective refractive, we select five common glass materials for the claddings in the PCF, namely SiO_2, amethyst, SSK2, SF11, and LaSF09. When the wavelength is 1.55 μm, the refractive index of these five materials increases gradually in the above order, so that the influence on the performance of OAM modes for cladding materials with different refractive indices can be determined.

SiO_2 has been widely used in optical fibers for its good physical and chemical properties. It is possible to inlay amethyst in SiO_2 because the melting point of amethyst [25] is higher than that of SiO_2. It not only improves the effective refractive index difference between adjacent modes, but also improves the number of OAM modes that can be stably transmitted. The SSK2 [36] heavy crown glass is a common material used to manufacture optical devices because the material dispersion at 1.55 μm is small. In addition, because its melting point is lower, the difficulty encountered in the actual drawing process of the PCF decreases. LaSF09 [20] is a lanthanum dense flint optical glass which is an environmental protection substitute for the traditional lead and arsenic containing glass. Its average refractive index in the visible and near-infrared regions is higher than that of common glass. The effective refractive indices of SiO_2, SSK2, SF11, and LaSF09 can be derived by the Sellmeier equation [37] and the values of A_1, A_2, A_3, B_1, B_2, and B_3 are shown in Table 1:

$$n^2(\lambda) = 1 + \frac{A_1\lambda^2}{\lambda^2 - B_1} + \frac{A_2\lambda^2}{\lambda^2 - B_2} + \frac{A_3\lambda^2}{\lambda^2 - B_3}. \tag{4}$$

The refractive index of amethyst depends on the single Sellmeier equation [38]:

$$\frac{1}{n^2 - 1} = -\frac{A}{\lambda^2} + B, \tag{5}$$

where $A = 0.0065$ and $B = 0.7359$. In order to discuss the effects of the cladding materials on the performance of OAM optical fiber communication more appropriately, it is important to choose the suitable optical fiber structure. OAM modes are generally distributed in hollow structures with an annular region and so we design a large air hole in the center of the PCF and a circular area for OAM mode transmission. The air hole not only determines the confinement loss of OAM mode propagation in the PCF, but also is a key factor to restrict light in the ring region. As a result, the proper air hole arrangement is necessary for stable transmission of OAM modes. In addition, to match the structure of vortex rotation, the air holes should be arranged as a ring and the number of holes ought to be as large as possible because photons can be better bound in the annular region to minimize leaking to the cladding. Consequently, the layers and number of air holes are important physical quantities that affect the performance of OAM mode transmission.

Figure 1 shows the selected structure in which the center is a large air hole with a radius of R_0 optimized in the range of $4.5\ \mu m < R_0 < 5.2\ \mu m$. With increasing R_0, the number of OAM modes increases gradually. However, when $R_0 > 5\ \mu m$, the optical field of the OAM mode is distorted and when R_0 is less than 5 μm, the number of OAM modes transmitted in the PCF decreases. Therefore, the obtained law does not have a strong universal nature and so R_0 is set to be 5 μm. The thickness of the annular region ($R_1 - R_0$) is an important structural parameter which affects dispersion of OAM modes. When $R_1 - R_0 = 2\ \mu m$, the OAM modes have the lowest and flat waveguide dispersion and so $R_1 = 7\ \mu m$. The air holes with a diameter d are distributed evenly outside the annular region and the size of the air holes determines photon leakage into the cladding. We optimize d in the range of 1.5–1.8 μm. When $d = 1.6\ \mu m$, the light field distribution of the OAM mode is the most concentrated and leakage is the least. It should be noted that when $d < 1.6\ \mu m$, the quantity of air holes on the first level increases, which is not conducive to PCF production and therefore, d is set to be 1.6 μm. The arrangement of air holes has a significant impact on the confinement loss of OAM modes. According to the optimization method, setting the air holes with the same number and size of two layers and layer spacing of 0.15 μm can minimize the loss of OAM modes. When the cladding radius $R_2 = 10.4\ \mu m$, there is no high-order radial mode in the PCF. The perfect matching layer represented by the green region can absorb all the radiation and provide the ideal boundary conditions. In summary, we set $R_0 = 5.0\ \mu m$, $R_1 = 7.0\ \mu m$, $R_2 = 10.4\ \mu m$, $a = 0.15\ \mu m$, and $d = 1.6\ \mu m$.

This structure can be manufactured by the solgel method [39,40]. Under the action of catalyst, the material powder is

Table 1. Sellmeier Constants of SiO_2, SSK2, SF11, and LaSF09

	A_1	A_2	A_3	B_1	B_2	B_3
SiO_2	0.69616	0.4079426	0.897479	0.068404	0.1162414	9.896161
SSK2	1.4306027	0.153150554	1.01390904	0.00823982975	0.0333736841	106.870822
SF11	1.7384840	0.31116897	1.1749087	0.0136068604	0.061596046	121.922711
LaSF09	2.0002954	0.29892688	1.8069184	0.0121426017	0.061596046	121.922711

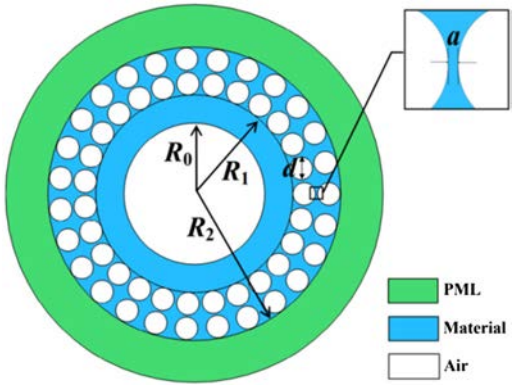

Fig. 1. Cross section of the PCF.

evenly mixed. It synthesizes a stable solgel system through the hydrolysis condensation method, and gel is formed by cooling and aging. The gel is dried to remove the solvent. Then, the background material powder is made into fiber preforms under gel heat treatment (900°C–1500°C), and then the fiber is drawn through melt quenching.

3. RESULTS AND DISCUSSION

A. Propagating Modes

The light field distribution reflects the performance of OAM mode transmission as shown in Figs. 2(a)–2(j), which discloses the light field distributions of some OAM modes transmitted by the PCFs with different background materials in the Z direction at 1.55 μm. The field distributions of all the eigenmodes are well confined in the respective annular regions. The light field distributions of the HE and EH modes are close to the cladding and core, respectively, and it is the most direct method to distinguish the HE and EH modes. The phase distributions of some OAM modes are shown in Figs. 2(k)–2(o).

B. Effective Refractive Index

The effective refractive index of the optical fiber can be defined as the average refractive index weighted by the light intensity distribution [41]. The effective refractive indices of all the HE modes and EH modes for different cladding materials at 1.55 μm are presented in Figs. 3(a) and 3(b).

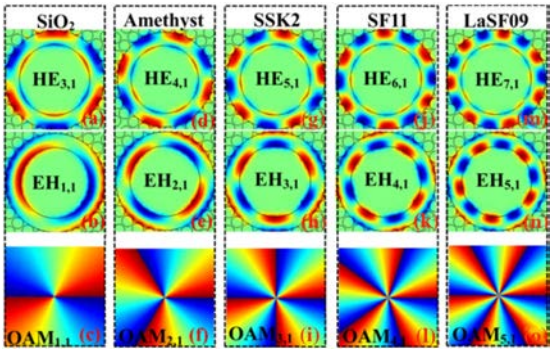

Fig. 2. (a)–(j) Optical field distributions of a part of the HE and EH modes in the zz direction; (k)–(o) phase diagrams of the partial HE and EH modes.

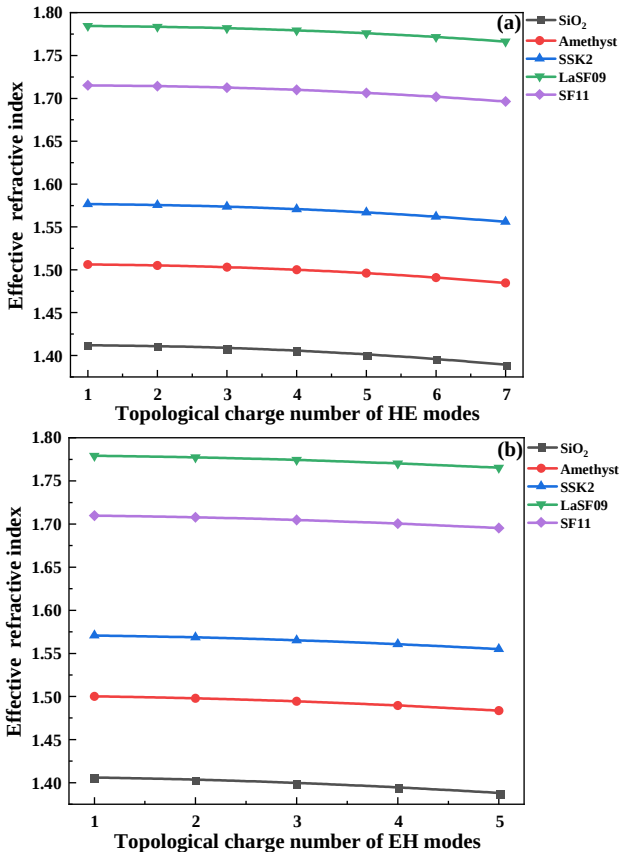

Fig. 3. Relationship between the effective refractive indices of (a) HE and (b) EH modes and topological charge number.

Figure 3 shows that with increasing topological charge, the effective refractive indices of the HE mode and EH mode decrease at 1.55 μm, which is because higher-order modes are more likely to leak into the cladding. The effective refractive index of HE and EH modes is much higher than other materials when the background material of the optical fiber is LaSF09, and the maximum effective refractive index obtained is 1.78 at $HE_{1,1}$. The effective refractive index of HE mode synthesized is greater than that of EH mode from the same order OAM mode, which is another method to distinguish HE mode from EH mode. The effective index difference of all the OAM modes for each fiber cladding material is shown in Fig. 4. Obviously, all of them are greater than 1×10^{-4} and the maximum effective refractive index differences of the five materials are 2.84×10^{-3}, 2.90×10^{-3}, 2.87×10^{-3}, 2.60×10^{-3}, and 2.71×10^{-3}, all obtained in OAM2,1, respectively. This proves that mode coupling in the PCF is quite low and all OAM modes can be transmitted stably over a long distance. In addition, the reason why the effective index difference is negatively correlated with the topological charge is that increasing the topological charge changes the OAM mode gradually into a high-order mode. Moreover, the ability of the annular region to limit the photon in the mode field is weakened, thereby making the photon energy of the mode synthesized by the same order OAM mode leak to the cladding, while the energy of the EH mode is almost unchanged.

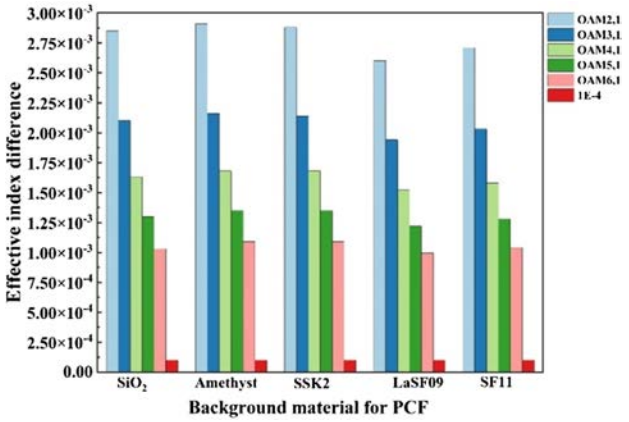

Fig. 4. Effective refractive index difference of the HE and EH modes.

C. Chromatic Dispersion

Dispersion is one of the parameters affecting transmission in optical fibers. Optical pulse broadening is caused by different velocities of different frequencies in the spectral components of the light source in the PCF [42]. The total dispersion of PCF is composed of materials dispersion and waveguide dispersion. Waveguide dispersion is caused by different phase constants and group velocities of a certain waveguide mode in the fiber at different frequencies. The dispersion of materials is determined by their own characteristics. The effective refractive index of materials is related to frequency in PCF, $n = \sqrt{\mu_r \varepsilon_r}$, μ_r is the relative permeability which is 1 among the five materials selected in this work, and $\varepsilon_r = \varepsilon_r(\omega)$ is relative permittivity related to wavelength and it is the main cause of material dispersion. When calculating the effective refractive index, the influence of material dispersion is already included; as a result, waveguide dispersion dominates the total dispersion. The total dispersion can be calculated by Eq. (6) [43]:

$$D = D_m + D_w = -\frac{\lambda}{c}\frac{d^2 \mathrm{Re}(n_{\mathrm{eff}})}{d\lambda^2}, \tag{6}$$

where D_m and D_w are the materials and waveguide dispersion, n_{eff} is the real part of the effective refractive index of the OAM modes, and c is the speed of light in vacuum medium. Table 2 shows the materials dispersion for the five cladding materials at 1.55 μm.

Figures 5(a) and 5(b) show the dispersion of the HE and EH modes, respectively. The dispersion of the OAM modes of the five materials is positively related to the topological charge number, because as the topological charge increases, the limiting ability of the annular region on field strength weakens gradually, and more photons diffuse into the cladding. The minimum

Table 2. Materials Dispersion of the Five Materials at 1.55 μm

Material	SiO_2	Amethyst	SSK2
D_m[ps/(nm·km)]	−313.91	−212.33	−321.79
Material	**SF11**	**LaSF09**	
D_m[ps/(nm·km)]	−33.277	− 772.08	

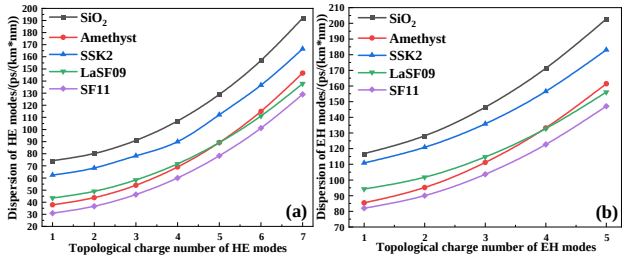

Fig. 5. Dispersion trend of (a) HE and (b) EH modes with changing topological charge numbers.

dispersion of the OAM modes is 30.95 ps/(nm · km) at $HE_{1,1}$ when the background material is SF11. The maximum dispersion is 202.73 ps/(nm · km) when the background material is SiO_2. This is because the propagation frequency is the largest when photons are transmitted in the PCF with SiO_2 as the cladding material, resulting in the highest optical pulse broadening. Consequently, photons limited in the annular region are the least and dispersion is the largest.

D. Effective Mode Area and Nonlinear Coefficient

The effective mode area represents the concentration of photon energy, and a larger mode field area improves the stability of OAM mode transmission in optical fibers [20]. The nonlinear effect in optical fiber is caused by the change of refractive index of the medium with light intensity, inelastic scattering, and power dependence of refractive index, including self-phase modulation, cross-phase modulation, and four-wave mixing. The nonlinear polarization of the medium under the action of strong light will cause nonlinear effects, which will make the parameters of the fiber change nonlinearly and have a negative impact on the OAM modes [44]. The nonlinear coefficient is a physical quantity to measure the nonlinear effect and is inversely proportional to the effective mode area. The larger the effective mode field area, the smaller the nonlinear coefficient, the higher the communication efficiency of the optical fiber, and the better the transmission characteristics of OAM modes. The effective mode area and corresponding nonlinear coefficient can be obtained from Eqs. (7) and (8) [29]:

$$A_{\mathrm{eff}} = \frac{\left(\iint |E(x,y)|^2 \mathrm{d}x\mathrm{d}y\right)^2}{\iint |E(x,y)|^4 \mathrm{d}x\mathrm{d}y}, \tag{7}$$

$$\gamma = \frac{2\pi n_2}{\lambda A_{\mathrm{eff}}}, \tag{8}$$

where $E(x, y)$ is the electric field distribution and n_2 is the nonlinear refractive index of the five cladding materials. n_2 can be obtained as [45]

$$n_2 = \frac{K(n_d - 1)\left(n_d^2 + 2\right)^2}{v_d\left[1.517 + \frac{(n_d^2+2)(n_d+1)}{6n_d}v_d\right]^{\frac{1}{2}}} 10^{-13}, \tag{9}$$

where K is an empirical factor which is 9×10^{-6}, n_d is the linear refractive index, and v_d is the Abbe number. n_d and v_d of the five cladding materials can be found in [46]. Table 3 shows the nonlinear refractive indices of the five materials.

Table 3. Nonlinear Refractive Indices of the Five Materials

Material	SiO_2	Amethyst	SSK2
n_2	2.3×10^{-20}	2.6×10^{-20}	1.7×10^{-20}
Material	**SF11**	**LaSF09**	
n_2	1.68×10^{-20}	2.0×10^{-20}	

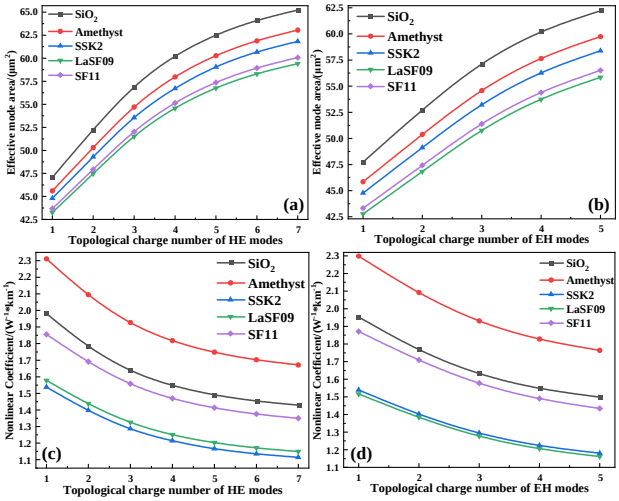

Fig. 6. Effective mode areas of (a) HE and (b) EH modes; nonlinear coefficients of (c) HE and (d) EH modes.

Figures 6(a)–6(d) describe the effective mode field areas and nonlinear coefficients of the OAM modes with different topological charge numbers for the five materials. Figures 6(a) and 6(b) reveal that with increasing number of OAM modes, more photons leak into the cladding and the effective mode area is thus proportional to the number of topological charges. In addition, the OAM modes show the smallest effective mode area (42.78 μm^2) as the cladding is made of LaSF09. When the background material is SiO_2, the effective mode area of the HE and EH modes is the largest, and the maximum value is 65.23 μm^2 at $HE_{7,1}$. This is because LaSF09 has the highest effective refractive index, strongest light limiting ability in the fiber energy concentration area, and lowest number of photons diffusing into the cladding. Figures 6(c) and 6(d) show that the nonlinear coefficients are negative feedback to the topological charge. Moreover, the nonlinear coefficients of eigenmodes transmitted in the PCF with SSK2 and LaSF09 background materials are lower than those of other background materials in PCF, which means that these two materials perform well in suppressing the nonlinearity effect.

E. Numerical Aperture

The NA is an important dimensionless physical quantity in optical fiber transmission reflecting the level of photons received by the end of the optical fiber and playing a key role in the coupling efficiency between the optical fiber and light source [47]. The NA is related to the refractive index of the core and relative index difference between the core and cladding. It can be computed by the following expression [48]:

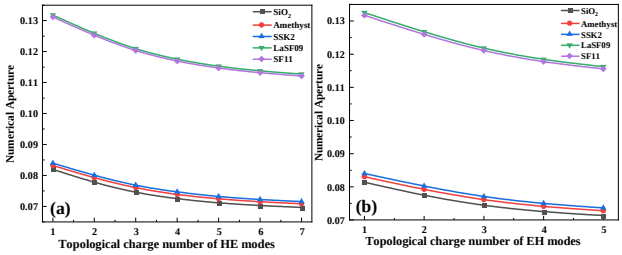

Fig. 7. Variation trend of the numerical aperture with topological charge number of (a) HE and (b) EH modes.

$$\mathrm{NA} = \left(1 + \frac{\pi A_{\mathrm{eff}}}{\lambda^2}\right)^{\left(-\frac{1}{2}\right)}. \tag{10}$$

Figures 7(a) and 7(b) indicate that the NA decreases with increasing topological charge, for the reason that when the number of OAM modes increases, it becomes more difficult for the fiber to receive photons and photons leak into the cladding more frequently. The NA of the EH modes is the largest if the cladding is made of LaSF09 and it is 0.133 when $l = 1$. This is because the refractive index of the fiber core is the largest and the optical fiber shows the best effects of receiving photons. The minimum NA was obtained at $EH_{5,1}$ when the background material of the PCF was SiO_2, which is 0.071. From the perspective of increasing the optical power entering the fiber, it is most advantageous for fiber docking when the background material of the PCF is LaSF09. However, when the NA value is too large, the mode distortion of the fiber also increases, which will affect the bandwidth of the fiber.

F. OAM Purity

OAM purity is a momentous parameter to be considered when the PCF is used for optical communication because only the modes with high purity can propagate stably in the fiber and it reduces the difficulty of demultiplexing the optical fiber at the output end. In addition, high mode purity reduces confinement loss and increases signal propagation distance. The mode purity is defined by the following formula [28]:

$$\eta = \frac{I_r}{I_c} = \frac{\iint_{\mathrm{ring}} |E|^2 \mathrm{d}x\mathrm{d}y}{\iint_{\text{cross-section}} |E|^2 \mathrm{d}x\mathrm{d}y}, \tag{11}$$

where I_r is the average light intensity of the annular region containing all the OAM modes and I_c is the average light intensity of the cross-sectional region in the PCF. Figures 8(a) and 8(b) show that the mode purity is inversely proportional to the topological charge of the HE mode and directly proportional to the topological charge of the EH mode. This is because the HE mode is closer to the cladding, more photons leak into the cladding as the mode order increases, while the EH mode is closer to the core, and the annular region has a stronger restriction on photons. Obviously, OAM purity of all eigenmodes is higher than that of other background materials as the background material of PCF is made of LaSF09, with a maximum value = 0.98 at $HE_{1,1}$. It indicates that the OAM mode has the highest transmission stability when LaSF09 is used as the cladding material. OAM mode purity is lowest with SiO_2 as the

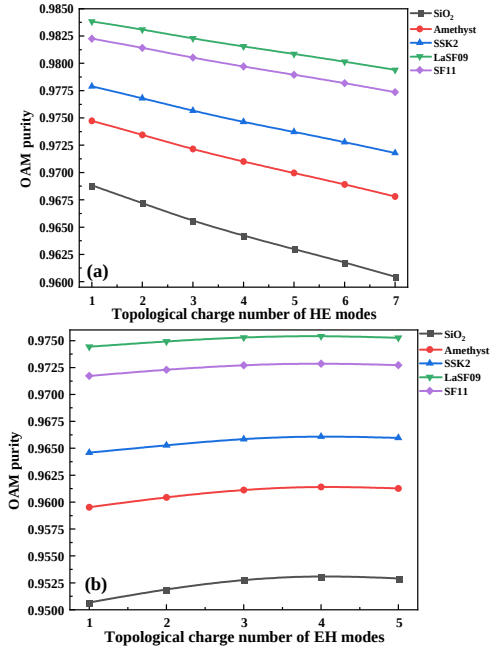

Fig. 8. OAM purity of the (a) HE and (b) EH modes.

background material; the minimum value is 0.95 ($EH_{1,1}$). This represents that LaSF09 has better potential for long-distance stable transmission than SiO_2.

G. Confinement Loss

The confinement loss has a great impact on the overall loss [29] and is a unique loss of photonic crystal fibers due to their own structure. Due to the unique structure of PCF, the limiting ability of air holes with different sizes and arrangements to light intensity is distinct, and the air holes in the cladding are restricted. When OAM modes transmit in PCF, some field strength will leak into the cladding from the annular region, resulting in losses. The extent of confinement loss is related to the structural parameters of PCF and wavelength and is an important parameter for measuring the performance of PCF. It can be obtained from the imaginary part of the effective refractive index by Eq. (12) [49]:

$$L = \frac{2\pi}{\lambda}\frac{20}{\ln(10)}10^6 \mathrm{Im}(n_{\mathrm{eff}}), \tag{12}$$

where $\mathrm{Im}(n_{\mathrm{eff}})$ is the imaginary part of the effective refractive index and λ is the wavelength. Figures 9(a) and 9(b) show that the confinement loss increases gradually with increasing topological charge, because the ability of a light field to control photon energy is negatively correlated with the order of the OAM mode in optical transmission. The minimum confinement loss for all eigenmodes is 9.98×10^{-6} (dB/m) when the background material is LaSF09. In addition, the confinement loss of SiO_2 is much greater than that of the other materials because photons tend to transmit in the medium with a large refractive index. SiO_2 has the smallest effective refractive index among the five materials, and photons have a greater tendency to move in the high-refractive-index media resulting in the largest number of photons leaking into the cladding. This indicates

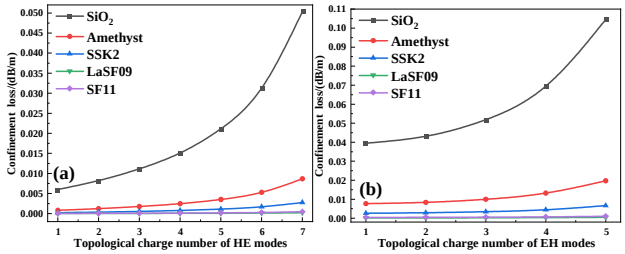

Fig. 9. Patterns of confinement loss of (a) HE and (b) EH modes with changing topological charge numbers.

that the PCF background material of LaSF09 is more suitable for stable transmission over long distances in optical fiber.

H. Walk-Off Length

When the fast and slow OAM modes generate a certain distance in transmission, the interaction between the two modes will no longer occur [50]. Once the distance between odd and even modes for composing the OAM mode with the identical order is too large, the OAM mode will not be synthesized thus resulting in spatial walk-off. A 10 ps walk-off length is a physical quantity to describe the degree of walk-off effect and it is inversely proportional to modal birefringence, as shown by Eq. (13) [31]:

$$L_{10\,\mathrm{ps}} = \frac{c \times 10\ \mathrm{ps}}{n_{\mathrm{eff}}^{\mathrm{even}} - n_{\mathrm{eff}}^{\mathrm{odd}}} = \frac{3 \times 10^{-3}}{n_{\mathrm{eff}}^{\mathrm{even}} - n_{\mathrm{eff}}^{\mathrm{odd}}}(m), \tag{13}$$

where $L_{10\,\mathrm{ps}}$ and c are the 10 ps walk-off length and speed of light, respectively, and $n_{\mathrm{even}}^{\mathrm{eff}}$ and $n_{\mathrm{odd}}^{\mathrm{eff}}$ represent the effective refractive indices of the even and odd modes. Figures 10(a) and 10(b) describe the 10 ps walk-off length of the HE and EH

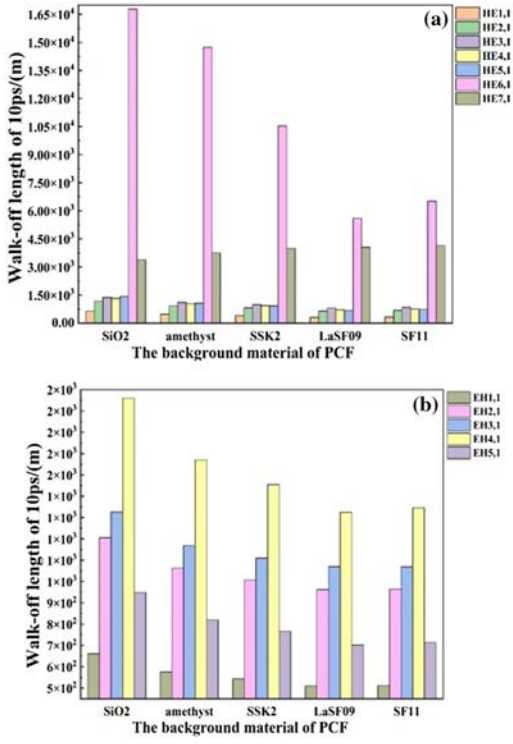

Fig. 10. Relationship between the walk-off lengths of (a) HE and (b) EH modes and topological charge numbers.

modes for the five materials. It should be noted that the walk-off length does not change regularly with topological charge. The walk-off length of the EH modes increases gradually with increasing topological charge up to $l = 4$ and then decreases when $l = 5$. For the HE modes, the walk-off length reaches a peak compared with other topological charges when the topological charge is 6. The maximum value is 1.68×10^4 m ($HE_{1,1}$) when the cladding is composed of SiO_2, which expresses that the mode can stably transmit the farthest distance in optical fibers. It is very conducive to long-distance signal transmission.

I. Evaluation of Structure Parameter Deviation from Design

In manufacturing, the structure parameters of PCF inevitably result in partly error compared to the designed parameters. Therefore, this paper evaluates the deviation of each parameter of the proposed PCF from design. During transmission, confinement loss is the decisive factor determining the transmission distance and characteristics of OAM modes in PCF. Therefore, the impact of structure parameter deviation generated in actual production of PCF on transmission performance can be researched based on confinement loss. Figures 11(a)–11(e) describe the influence of tiny changes in the radius of the central air hole, the thickness of the annular area, the diameters of two layers of air holes in the annular region, and the spacing of air holes on confinement losses in production.

Figure 11(e) depicts that the confinement loss remains almost unchanged with the variation of space of air holes, indicating that fabrication error of air holes has little effect on confinement loss. Although changes in other structure parameters have influence on confinement losses, the amount of variation is very tiny. Its maximum variation is 3.66×10^{-4} dB/m, obtained when the radius of the central air hole changes at $EH_{5,1}$. Therefore, Figs. 11(a)–1(e) demonstrate that the devised PCF has excellent tolerance and is suitable for production.

J. Comparison of OAM Communication Performances in the Literature

The performance comparison of dispersion, effective mode area, nonlinear coefficient, numerical aperture, and mode purity shown in Table 4 indicates that the proposed PCF has significant advantages in terms of dispersion, effective mode field area, and nonlinear coefficient after replacing the background material. In addition, although the numerical aperture and mode purity are relatively low compared to [23,51], they still have excellent OAM transmission characteristics within the allowable range. Consequently, the new optical fiber material exploited in this work can effectively improve the performance of OAM modes, providing a theoretical basis for high quality and efficient transmission of OAM modes in PCF in the future.

4. CONCLUSION

By adopting a simple PCF structure that supports OAM modes, we study the effects of the effective refractive index, nonlinear coefficient, OAM purity, walk-off length, and other parameters

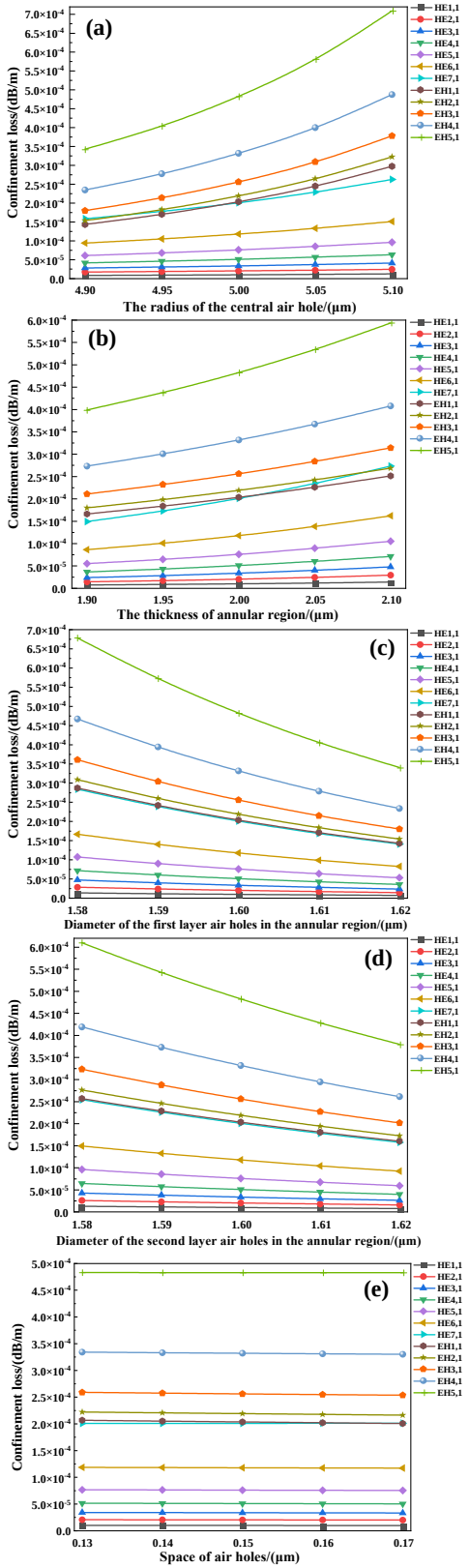

Fig. 11. Influence of changes in (a) the radius of the central air hole, (b) the thickness of annular area, (c) the diameters of first-layer air holes in the annular region, (d) the diameters of second-layer air holes in the annular region, and (e) the spacing of air holes on confinement losses.

Table 4. Comparison in OAM Communication Performances with Other Reports

Refs.	Dispersion/ps/(nn·km)	Effective Mode Area/(μm^2)	Nonlinear Coefficient/($W^{-1}\cdot km^{-1}$)	Numerical Aperture	OAM Purity
[51]	33.28	26.24	—	0.28	—
[23]	52.37	48.43	2.18	—	0.99
[3]	73.43	26.93	3.98	—	—
[52]	73.58	50.54	2.08	—	—
This work	30.95	65.23	1.11	0.13	0.98

on transmission of OAM modes for claddings made of five different materials of SiO_2, amethyst, SSK2, SF11, and LaSF09. Numerical analysis indicates that materials with a larger effective refractive index not only reduce dispersion and confinement loss of the OAM modes and make the transmission distance longer, but also increase the effective mode area and OAM purity to enhance the transmission stability of OAM modes. The results provide guidance to realize high-quality communication.

Funding. Scientific Research Fund of Sichuan Province Science and Technology Department (2020YJ0137); City University of Hong Kong Donation Research (No. 9229021); City University of Hong Kong Strategic Research Grant (SRG) (7005505); China Postdoctoral Science Foundation funded project (2020M670881); Local Universities Reformation and Development Personnel Training Supporting Project from Central Authorities, the Natural Science Foundation of Heilongjiang Province (LH2021F007).

Acknowledgment. This work was jointly supported by the Local Universities Reformation and Development Personnel Training Supporting Project from Central Authorities, the Natural Science Foundation of Heilongjiang Province, China Postdoctoral Science Foundation funded project, City University of Hong Kong Strategic Research Grant (SRG), City University of Hong Kong Donation Research Grant, and Scientific Research Fund of Sichuan Province Science and Technology Department.

Disclosures. The authors declare no conflicts of interest.

Data availability. Data underlying the results presented in this paper are not publicly available at this time but may be obtained from the authors upon reasonable request.

REFERENCES

1. M. Arumugam, "Optical fiber communication—an overview," Pramana **57**, 849–869 (2001).
2. R. G. Smith and S. D. Personick, "Receiver design for optical fiber communication systems," in *Semiconductor Devices for Optical Communication* (Springer, 1980), pp. 89–160.
3. H. Zhang, W. Zhang, L. Xi, X. Tang, X. Zhang, and X. Zhang, "A new type circular photonic crystal fiber for orbital angular momentum mode transmission," IEEE Photonics Technol. Lett. **28**, 1426–1429 (2016).
4. S. Weinstein and P. Ebert, "Data transmission by frequency-division multiplexing using the discrete Fourier transform," IEEE Trans. Commun. Technol. **19**, 628–634 (1971).
5. R. S. Tucker, G. Eisenstein, and S. K. Korotky, "Optical time-division multiplexing for very high bit-rate transmission," J. Lightwave Technol. **6**, 1737–1749 (1988).
6. A. D. Ellis, "The nonlinear Shannon limit and the need for new fibres," Proc. SPIE **8434**, 106–115 (2012).
7. L. F. Stokes, M. Chodorow, and H. J. Shaw, "All-single-mode fiber resonator," Opt. Lett. **7**, 288–290 (1982).
8. Q. Wang, G. Farrell, and W. Yan, "Investigation on single-mode–multimode–single-mode fiber structure," J. Lightwave Technol. **26**, 512–519 (2008).
9. L. Cohen, "Comparison of single-mode fiber dispersion measurement techniques," J. Lightwave Technol. **3**, 958–966 (1985).
10. S. Berdagué and P. Facq, "Mode division multiplexing in optical fibers," Appl. Opt. **21**, 1950–1955 (1982).
11. N. Bozinovic, S. Golowich, P. Kristensen, and S. Ramachandran, "Control of orbital angular momentum of light with optical fibers," Opt. Lett. **37**, 2451–2453 (2012).
12. N. Bozinovic, Y. Yue, Y. Ren, M. Tur, P. Kristensen, H. Huang, A. E. Willner, and S. Ramachandran, "Terabit-scale orbital angular momentum mode division multiplexing in fibers," Science **340**, 1545–1548 (2013).
13. Z. Xie, S. Gao, T. Lei, S. Feng, Y. Zhang, F. Li, J. Zhang, Z. Li, and X. Yuan, "Integrated (de) multiplexer for orbital angular momentum fiber communication," Photonics Res. **6**, 743–749 (2018).
14. H. Zhang, X. Zhang, H. Li, Y. Deng, L. Xi, X. Tang, and W. Zhang, "The orbital angular momentum modes supporting fibers based on the photonic crystal fiber structure," Crystals **7**, 286 (2017).
15. D. Cozzolino, D. Bacco, B. Da Lio, K. Ingerslev, Y. Ding, K. Dalgaard, P. Kristensen, M. Galili, K. Rottwitt, S. Ramachandran, and L. K. Oxenløwe, "Orbital angular momentum states enabling fiber-based high-dimensional quantum communication," Phys. Rev. Appl. **11**, 064058 (2019).
16. C. Jia, H. Jia, N. Wang, J. Chai, X. Xu, Y. Lei, G. Liu, Y. Peng, and J. Xie, "Theoretical analysis of a 750-nm bandwidth hollow-core ring photonic crystal fiber with a graded structure for transporting 38 orbital angular momentum modes," IEEE Access **6**, 20291–20297 (2018).
17. N. Wang, J. L. Xie, H. Z. Jia, and M. M. Chen, "A low confinement loss double-photonic crystal fibre over 850 nm bandwidth with 26 orbital angular momentum modes transmission," J. Mod. Opt. **65**, 2060–2064 (2018).
18. T. He and B. Wu, "Low confinement loss photonic crystal fibre capable of supporting 54 orbital angular momentum modes," J. Mod. Opt. **67**, 556–562 (2020).
19. J. Yang, H. Zhang, X. Zhang, Z. Chen, L. Xi, and W. Zhang, "A hollow-core circular photonic crystal fiber mode selective coupler for generating orbital angular momentum modes," Opt. Fiber Technol. **64**, 102543 (2021).
20. H. Fu, M. Zhu, C. Liu, Z. Yi, J. Lv, L. Yang, F. Wang, Q. Liu, W. Su, X. Li, and P. K. Chu, "Photonic crystal fiber supporting 394 orbital angular momentum modes with flat dispersion, low nonlinear coefficient, and high mode quality," Opt. Eng. **61**, 026111 (2022).
21. W. Gao, W. Jiang, L. Tong, W. Dai, S. Liu, W. Chen, Z. Zhang, X. Ma, Y. Zhou, W. Zhang, W. Fang, and M. Liao, "Toward generation of mid-infrared orbital angular momentum beams by tailoring four-wave mixing in chalcogenide photonic crystal fiber," J. Opt. Soc. Am. A **38**, 692–698 (2021).
22. X. Wan, Z. Wang, B. Sun, and Z. Zhang, "Low dispersion and confinement loss photonic crystal fiber for orbital angular momentum mode transmission," Opt. Quantum Electron. **52**, 289 (2020).
23. L. Zhang and Y. Meng, "Design and analysis of a photonic crystal fiber supporting stable transmission of 30 OAM modes," Opt. Fiber Technol. **61**, 102423 (2021).
24. H. Fu, Y. Shi, Z. Yi, C. Liu, X. Song, J. Lv, L. Yang, and P. K. Chu, "Effects of air holes in the cladding of photonic crystal fibers on dispersion and confinement loss of orbital angular momentum modes," Opt. Quantum Electron. **54**, 353 (2022).
25. H. Fu, C. Liu, C. Hu, L. Zhou, Y. Shi, J. Lv, L. Yang, and P. K. Chu, "Circular photonic crystal fiber supporting 118 orbital angular momentum modes transmission," Opt. Eng. **60**, 076102 (2021).
26. A. N. Kolyadin, G. K. Alagashev, A. D. Pryamikov, L. Mouradian, A. Zeytunyan, H. Toneyan, A. F. Kosolapov, and I. A. Bufetov, "Negative

curvature hollow-core fibers: dispersion properties and femtosecond pulse delivery," Phys. Proc. **73**, 59–66 (2015).
27. G. Ruffini, M. D. Fox, O. Ripolles, P. C. Miranda, and A. Pascual-Leone, "Optimization of multifocal transcranial current stimulation for weighted cortical pattern targeting from realistic modeling of electric fields," Neuroimage **89**, 216–225 (2014).
28. H. Fu, C. Liu, Z. Yi, X. Song, X. Li, Y. Zeng, J. Wang, J. Lv, L. Yang, and P. K. Chu, "A new technique to optimize the properties of photonic crystal fibers supporting transmission of multiple orbital angular momentum modes," J. Opt. **52**, 307–316 (2023).
29. X. Ke and S. Wang, "Design of photonic crystal fiber capable of carrying multiple orbital angular momentum modes transmission," Opt. Photonics J. **10**, 49–63 (2020).
30. M. A. Kabir, M. M. Hassan, K. Ahmed, M. S. Mani Rajan, A. H. Aly, M. N. Hossain, and B. K. Paul, "Novel spider web photonic crystal fiber for robust mode transmission applications with supporting orbital angular momentum transmission property," Opt. Quantum Electron. **52**, 331 (2020).
31. C. Liu, H. Fu, C. Hu, L. Zhou, Y. Shi, J. Lv, L. Yang, and P. K. Chu, "Optimization of photonic crystal fibers for transmission of orbital angular momentum modes," Opt. Quantum Electron. **53**, 1 (2021).
32. S. M. Barnett, M. Babiker, and M. J. Padgett, "Optical orbital angular momentum," Philos. Trans. R. Soc. A **375**, 20150444 (2017).
33. S. F. Liew, H. Noh, J. Trevino, L. D. Negro, and H. Cao, "Localized photonic band edge modes and orbital angular momenta of light in a golden-angle spiral," Opt. Express **19**, 23631–23642 (2011).
34. W. Wang, N. Wang, and H. Jia, "Research on the dispersion characteristics of silica-based ring-core photonic crystal fiber used to transmit orbital angular momentum modes," Optik **241**, 166935 (2021).
35. J. Zhu, X. Wang, Y. Qi, and J. Yu, "Self-reference plasmonic sensor based on functional layer film composed of Au/Si gratings," Chin. Phys. B **31**, 014206 (2021).
36. I. Gotoh, M. Adachi, and E. Nishida, "Identification and characterization of a novel MAP kinase kinase kinase, MLTK," J. Biol. Chem. **276**, 4276–4286 (2001).
37. C. Liu, J. Lü, W. Liu, F. Wang, and P. K. Chu, "Overview of refractive index sensors comprising photonic crystal fibers based on the surface plasmon resonance effect [Invited]," Chin. Opt. Lett. **19**, 102202 (2021).
38. R. D. Shannon, R. C. Shannon, O. Medenbach, and R. X. Fischer, "Refractive index and dispersion of fluorides and oxides," J. Phys. Chem. Ref. Data **31**, 931–970 (2002).
39. M. Ahabboud, T. Lamcharfi, F. Abdi, N. Hadi, F. Z. Ajyaje, and M. Haddad, "Effect of Cu doping on structural and dielectric properties of $Pb_{1-x}Cu_x$ ($Zr_{0.52}Ti_{0.48}$) O_3 (PCxZT)($0 \leq x \leq 0.2$) ceramics prepared by sol-gel method," Asian J. Chem **33**, 665–670 (2021).
40. V. V. Ravi Kanth Kumar, A. K. George, W. H. Reeves, J. C. Knight, P. St.J. Russell, F. G. Omenetto, and A. J. Taylor, "Extruded soft glass photonic crystal fiber for ultrabroad supercontinuum generation," Opt. Express **10**, 1520–1525 (2002).
41. X. Wang, J. Zhang, J. Zhu, Z. Yi, and J. Yu, "Refractive index sensing of double Fano resonance excited by nano-cube array coupled with multilayer all-dielectric film," Chin. Phys. B **31**, 024210 (2021).
42. Y. Ni, L. Zhang, L. An, J. Peng, and C. Fan, "Dual-core photonic crystal fiber for dispersion compensation," IEEE Photonics Technol. Lett. **16**, 1516–1518 (2004).
43. Q. Liu, W. Lu, Y. Sun, J. Lv, W. Liu, C. Liu, S. Tai, B. Li, J. Zhao, Y. Jiang, T. Sun, and P. K. Chu, "A novel photonic quasi-crystal fiber for transmission of orbital angular momentum modes," Optik **251**, 168446 (2022).
44. H. Fu, Z. Yi, Y. Shi, C. Liu, J. Lv, L. Yang, and P. K. Chu, "Circular anti-resonance fibre supporting orbital angular momentum modes with flat dispersion, high purity and low confinement loss," J. Mod. Opt. **68**, 784–791 (2021).
45. D. Lorenc, M. Aranyosiova, R. Buczynski, R. Stepien, I. Bugar, A. Vincze, and D. Velic, "Nonlinear refractive index of multicomponent glasses designed for fabrication of photonic crystal fibers," Appl. Phys. B **93**, 531–538 (2008).
46. M. J. Weber, *Handbook of Optical Materials* (CRC Press, 2002).
47. J. Pniewski, G. Stepniewski, R. Kasztelanic, B. Siwicki, D. Pierscinska, K. Pierscinski, D. Pysz, K. Borzycki, R. Stepien, M. Bugajski, and R. Buczynski, "High numerical aperture large-core photonic crystal fiber for a broadband infrared transmission," Infrared Phys. Technol. **79**, 10–16 (2016).
48. H. Xu, X. Wang, Q. Kong, and D. Peng, "High numerical aperture photonic crystal fiber with silicon nanocrystals core for optical coherence tomography," Optik **219**, 165000 (2020).
49. S. M. A. Razzak and Y. Namihira, "Tailoring dispersion and confinement losses of photonic crystal fibers using hybrid cladding," J. Lightwave Technol. **26**, 1909–1914 (2008).
50. M. Sharma, N. Borogohain, and S. Konar, "Index guiding photonic crystal fibers with large birefringence and walk-off," J. Lightwave Technol. **31**, 3339–3344 (2013).
51. D. Vigneswaran, M. S. M. Rajan, B. Biswas, A. Grover, K. Ahmed, and B. Kumar Paul, "Numerical investigation of spiral photonic crystal fiber (S-PCF) with supporting high order OAM modes propagation for space division multiplexing applications," Opt. Quantum Electron. **53**, 78 (2021).
52. W. Tian, H. Zhang, X. Zhang, L. Xi, W. Zhang, and X. Tang, "A circular photonic crystal fiber supporting 26 OAM modes," Opt. Fiber Technol. **30**, 184–189 (2016).